Chapter 6

Differential Release of Gaseous NO and NO_2 from Illuminated Nitrate-doped Water Ice

C. S. Boxe,[1] A. J. Colussi,[1]* M. R. Hoffmann,[1]* I. Perez,[2] and R. C. Cohen[2]

[1]W. M. Keck Laboratories, California Institute of Technology, Pasadena, CA 91125, and
[2]Department of Chemistry and Department of Earth and Planetary Sciences, University of California, Berkeley, California 94720

Abstract

NO and NO_2 temperature-programmed desorption rates, R_N and R_D respectively, were measured over $NaNO_3$-doped polycrystalline ice irradiated at $\lambda \sim 320$ nm as a function of the heating ramp, $\partial H = d\mathrm{T}/d\mathrm{t}$, and nitrate concentration between $-30 \leq \mathrm{T}/^{\circ}\mathrm{C} \leq 5$. R_N and R_D both increase with rising temperature. However, although $R_N << R_D$ throughout confirming that NO is a secondary photochemical product, R_N displays an early acceleration at ~ -20 °C, preceding a similar surge in R_D at ~ -10 °C. This phenomenon is ascribed to a separation mechanism based on the preferential retention of NO_2 vs. NO in the fluid nanolayers lining the open channels of micrograined ice aggregates as both gases diffuse outward. We briefly analyze the implications of present findings on snowpack photochemistry.

This Chapter has been submitted as a paper to the Journal of Physical Chemistry (2005).

Introduction

Deposition is a major sink for atmospheric nitrate.[1,2] A significant fraction of nitrate is deposited in snow-covered isolated regions, such as the Antarctic ice shelf. The horizontally-uniform nitrate concentrations measured in these locations, suggest global, remote atmospheric sources.[3,4] If nitrate levels were preserved within ice cores, they would supply data on Earth's paleoclimatic and paleoatmospheric composition.[5,6] On the other hand, there is mounting evidence that nitrate undergoes solar photolysis in the snowpack, producing NO_x (= NO + NO_2).[7-17] The implication of nitrate photolysis are three-fold: 1) photochemical processes could alter ice core records of other trace species (i.e., CO_2 and CH_4), which in turn, may affect the retrieval of past atmospheric conditions;[6,17] 2) nitrate photodecomposition is a source of NO_x and $^{\cdot}OH$ within snowpack interstitial air and to the overlying boundary layer;[16,18-20] 3) $^{\cdot}OH$ will oxidize organic matter contained in the snowpack.[19,20]

We investigated the photoproduction of NO_2, NO_2^-, and NO during the irradiation of μM and mM spray-frozen nitrate solutions and obtained evidence supporting similar photochemical rates and mechanisms in both the ice and aqueous phase.[21-23] It appears that the quasi-liquid layer (QLL), subsurface-subeutectic solutions, or nanoconfined water[24] play a pivotal role in these processes. Recently, we showed that the amounts of NO_2 photodesorbed during nitrate scale nonlinearly with the heating ramp (∂H), temperature, and $[NO_3^-]_o$.[25] NO_2 emission profiles also revealed several transitions associated with structural relaxations of the polycrystalline ice matrix.[25]

Here, we report measurements of NO and NO_2 fluxes during the temperature-programmed photolysis ($\lambda \geq 300$ nm) of nitrate-doped polycrystalline ice layers as a

function of $[NO_3^-]_o$ and ∂H based on chemiluminescence and laser-induced fluorescence (LIF) detection techniques, respectively, with pptv sensitivities.

Experimental Methods

As shown previously,[21,23] a schematic representation of the photo-reaction chamber, containing the reaction cell, is shown in Figure 6.1 (a) and 6.1 (b). 2 μM and 50 mM precooled $NaNO_3$ (EM Science) solutions at pH $\leq$ 6 were sprayed on a coldfinger (CF in Figure 6.1 (b), exposed area A = 304 cm^2), forming uniform nitrate-doped polycrystalline deposits. Ice coating temperatures were governed by an external cryogenic unit (Thermo Neslab ULT-80) with coolant fluid flowing through the coldfinger. The ice-encumbered CF was enfolded and sealed within a quartz sheath (QS). Compact-equivalent ice layers varied from 6.0 cm^3 to 13.25 cm^3 in volume, and from 197 μm to 436 μm in thickness.[26] This arrangement was then placed inside a reflective cylindrical stainless steel chamber (Figure 6.1 (a)), fitted with four Hg Pen-Ray UV lamps (UVP, modal 90-0001-04), emitting at $\lambda = 313 \pm 20$ nm, symmetrically positioned around the QS. The photon flux incident onto the QS, $I_i = 3.0 \times 10^{15}$ photons cm^2 s^{-1}, was determined by potassium ferrioxalate actinometry.[27] Ice matrices were subjected to variable temperature ramp rates (∂H = 0.70 ^oC min^{-1} and 0.10 ^oC min^{-1}) between $-30 \leq T/^oC \leq 5$ during irradiation and isothermal irradiation at −30, −20, −10, and −4 ^oC. Temperature ramp rates were controlled by a computer interfaced with the cryogenic unit that utilizes Thermo Neslab Nescom software. Lamp stability was monitored by a photocell (UDT Sensors, model PIN UV 100L), fixed atop the chamber. NO and NO_2

were carried to their detection systems, chemiluminescence, laser-induced fluorescence, respectively, by zero air flowing at 2.5 L min^{-1} through the QS-CF apparatus.

NO emissions were detected by chemiluminescence (Thermo Electron Corporation, Model 42C-TL NO-NO_2-NO_x Analyzer). This technique involves reacting ozone with the trace levels of photogenerated NO to produce electronically excited NO_2*, which emits a broad continuum from 500 to 2800 nm that peaks at 1300 nm.[28] A red-sensitive photomultiplier tube (PMT) is used to monitor the visible (500-900 nm) portion of this emission. A schematic representation of the chemiluminescence instrument in attached to the photoreactor is shown in Figure 6.2.

NO_2 was measured by laser-induced fluorescence.[29] A pulsed dye laser is utilized to tune on and off NO_2 resonance in close proximity to 585 nm. Total fluorescence is integrated from 750 nm to the long wavelength cutoff, $\lambda \sim 1100$ nm, of the GaAs PMT used for detection; this latter process occurs concurrently with the pulsed laser.[29] A schematic representation of the LIF instrument in conjunction with the nitrate photo-reaction chamber is shown in Figure 6.3.

Results and Discussion

Nitrate exhibits a weak absorption band (260-350 nm), centered at 302 nm (ε_{max} = 7.14 M^{-1} cm^{-1}).[30-33] The direct photolysis of nitrate in aerated aqueous solutions at $\lambda >$ 300 nm and pH < 6 is known to proceed through the following two primary reactions:[34-36]

$$NO_3^- + H^+ \xrightarrow{h\nu} NO_2 + {}^{\cdot}OH \quad (1)$$

$$NO_3^- \xrightarrow{h\nu} NO_2^- + O(^3P) \quad (2)$$

While approximately 90% of nitrate irradiation proceeds through reaction 1, 10% occurs through reaction 2.[37,38] Nitrite has two absorption bands in the UVB (290-320 nm) and UVA (320-400 nm) region, with an absorption maximum centered at 354 nm (ε_{max} = 22.7 M^{-1} cm^{-1}).[39-42] Photolysis of nitrite leads to the production of NO as shown below (eq. 3):

$$NO_2^- + H^+ \xrightarrow{h\nu} NO + {}^{\cdot}OH \qquad (3)$$

Therefore, the small branching ratio, R_2/R_1, in conjunction with the fact that NO derives from the photolysis of NO_2^-, reaction (3), result in $R_D/R_N \sim 2 - 30$ values in all experiments.[16]

Figures 6.4a and 6.4b display NO and NO_2 fluxes during the photolysis of $[NO_3^-]_o$ = 50 mM at ∂H = 0.70 and 0.10 ^oC min^{-1}, respectively. NO temperature-programmed desorption rates, R_N, markedly increase at ~ –20 ^oC, while NO_2 temperature-programmed desorption rates, R_D, only surge at ~ –10 ^oC. This puzzling observation (see above) can be rationalized by the larger affinity of NO_2(g) vs. NO(g) for the condensed phases. Henry's law coefficients, H, for NO_2 are approximately tenfold larger that those of NO in water between –30 ^oC and 5 ^oC [$H_{NO_2} = 6.67\times10^{-2}$ vs. $H_{NO} = 5.76\times10^{-3}$ M atm $^{-1}$ at - 30 ^oC; $H_{NO_2} = 1.84\times10^{-2}$ vs. $H_{NO} = 2.70\times10^{-3}$ M atm $^{-1}$ at 5 ^oC]. It is also known that the ice-air partition coefficients for NO and NO_2 are 1 × 10^{-3} and 3 × 10^{-3} at –27 ^oC, and 2 × 10^{-3} and 3 × 10^{-3} at –5 ^oC, respectively.[43] Therefore, as the NO and NO_2 photoproduced in the interior of the frozen nitrate solution exit into the overhead atmosphere via gas-phase diffusion through the open channel network of micrograined ice they will be retained by the wet (or dry)[43] ice/gas interfaces during a fraction of the time that is proportional to their corresponding Henry's law constants. This interpretation is validated by the post-illumination thermal desorption profiles of NO and NO_2 (Fig.

6.5). It is apparent that the ice matrix induces the differential desorption of both gases by a mechanism resembling chromatographic separation.

This phenomenon also shows that NO and NO_2's thermograms at ∂H = 0.70 and 0.10 $^oC\ min^{-1}$ are governed by a combination of processes. For example, during mM NO_3^- photolysis at ∂H = 0.70, 0.30, and 0.10 $^oC\ min^{-1}$, the overall emission profiles of NO_2 are determined by: 1) primary photolysis of NO_3^- (eq. 1);[34-36] 2) NO_2 secondary photolysis (eq. 6);[25] 3) solute effects on the premelting of ice interfaces;[21,25,44] 4) the delayed release of NO_2, trapped in closed subeutectic solution pockets until the structural relaxation of the topmost ice layers at higher temperatures;[21,25] 5) chemical losses due to radical reactions; and NO_2's most pronounced chemical loss pathway, its fast hydrolysis (eqs. 7 and 8).[25]

$$NO_2 \xrightarrow{h\nu} NO + O(^3P) \quad (6)$$

$$2\ NO_{2\,(aq)} + H_2O_{(l)} \rightarrow NO_3^-{}_{(aq)} + NO_2^-{}_{(aq)} + 2\ H^+{}_{(aq)} \quad (7)$$

$$2\ NO_{2\,(g)} + H_2O_{(l)} \rightarrow NO_3^-{}_{(aq)} + NO_2^-{}_{(aq)} + 2\ H^+{}_{(aq)} \quad (8)$$

Apart from the speed of NO molecules through the polycrystalline ice matrices, the photolysis of NO_2^- (eq. 3) and NO_2 (eq. 6), and the oxidation of NO by OH (eq. 9),[34] should dictate NO emission profiles during NO_3^- photolysis.

$$NO + OH \rightarrow HNO_2 \quad (9)$$

Figures 6.4a and 6.4b show that the production of NO dominate although NO is oxidized by OH (eq. 9). Since the dominant loss pathway for photoproduced NO_2 is fast via hydrolysis (eqs. 7 and 8)[25] and nitrite's steady-state concentration, $[NO_2^-]_{ss}$, during mM NO_3^- photolysis at –20 and –5 ^oC is reached at about 1.5 and 10 hrs, respectively,[22,23] we infer that the production of NO is controlled by the photolysis of

NO_2^- as NO_2^- concentrations rise toward steady-state (e.g., NO thermogram throughout at ∂H = 0.70 ^oC min^{-1} and NO thermogram at ∂H = 0.10 ^oC min^{-1} at T $\leq$ –20 ^oC). Afterwards (e.g., NO thermogram at ∂H = 0.10 ^oC min^{-1} at T > –20 ^oC), NO_2 photolysis will dictate NO production.

Figures 6.6a-c and 6.7a-c show isothermal emissions of NO and NO_2 for 1 hr at –30, –20, –10, and –4 ^oC, where the temperature of the polycrystalline ice matrices between isothermal irradiation (e.g., between –30 and –20 ^oC) were ramped at 0.70 ^oC min^{-1} with light (Fig. 6.6a-c) and without light (Fig. 6.7a-c). They display similar behavior for R_N and R_D, starting at ~ –20 and ~ –10 ^oC, respectively, during the irradiation of $[NO_3^-]_0$ = 50 mM. These additional experiments validate even more that the marked release of NO molecules, starting at lower temperatures, compared to NO_2, is likely due to the preferential partitioning of NO to air at the QLL and its faster movement in subsurficial water channels relative to NO_2.

Implications for Snowpack Chemistry in Polar Regions

The actual NO_3^- concentrations measured in snow-covered rural and remote regions range from 1 to 20 μM.[5,45-48] Since the lower range of nitrate, $[NO_3^-]_o$, embedded within our polycrystalline ice falls within the range of concentrations observed in field studies, our current results provide further evidence that the photolysis of nitrate in the upper portion of accumulated snow is a major source of NO_2 and NO_x to the overlying air masses.

For example, during the isothermal irradiation of $[NO_3^-]_o$ = 2 μM (Fig. 6.7c), we observed gas phase NO_2 concentrations that ranged from 100 pptv (F_{NO_2} = 5.0 × 10^8

molecule cm^{-3} s^{-1}) at –30 °C to 175 pptv (F_{NO_2} = 6.6 × 10^8 molecule cm^{-3} s^{-1}) at –4 °C. In comparison, Dibb *et al.*[10] measured NO_2 concentrations near 50 pptv at solar noon during snow chamber experiments in Greenland. In a separate study, Beine *et al.*[9] reported gas phase NO_2 concentrations that reached 30 pptv at solar noon over Alert, Canada within the Arctic Circle. In contrast, Jones *et al.*[14] reported levels of NO_2 up to 15 pptv over the Antarctic snowpack with a peak NO_2 production rate of 2.1 × 10^6 molecule cm^{-3} s^{-1}. In other work in the Antarctic, Cotter *et al.*[49] measured an average NO_2 production rate of (1.1 ± 0.3) × 10^7 molecule cm^{-3} s^{-1} over the temperature range of –30 to –20 °C in snow chamber experiments. More recent research conducted by Jacobi *et al.*[50] at the Summit site in Greenland showed NO_2 levels around 25 pptv at solar noon.

The relative differences between our experimental results for NO_2 fluxes and gas phase concentrations compared to those reported for the field measurements described above can be attributed to the role of other *in situ* reactions that may, in effect, control the observed ambient levels of NO_2 measured in the atmosphere over the snowpack. For example, Anastasio and Jordan[51] show recently that the photolysis of aerosol particles collected over the Arctic rapidly produce both ·OH (e.g., ~ 1 mM h^{-1}) and H_2O_2 (e.g., ~ 9 mM h^{-1}) when suspended in aqueous solution. In addition, they argue that the photolysis of hydrogen peroxide is the major source of hydroxyl radical in snow. Hydrogen peroxide, which is abundant in the surface layer of snow in polar regions, is readily photolyzed to produce ·OH.[52,53] With this in mind, the following reactions,

$$H_2O_2 \xrightarrow{h\nu} 2\,{\cdot}OH \qquad (10)$$

$$NO_2 + {\cdot}OH \longrightarrow HNO_3, \qquad (11)$$

coupled with the direct photolysis of NO_2 (eq. 12) in the interstitial air of the snowpack will be major sinks of NO_2 before release to the overlying atmosphere.

$$NO_2 \xrightarrow{h\nu} NO + {}^{\cdot}O(^3P) \quad (12)$$

The higher range of nitrate, $[NO_3^-]_o$, doped in our polycrystalline matrices lies within the range of NO_3^- concentrations (e.g., 4 to 23 mM) measured in mid-latitude snow-covered regions.[54-56] Therefore, the production of NO_2 and NO_x during nitrate photolysis and eventual release to the overlying air masses in these regions will occur. Recently, Fisher *et al.*[54] measured NO_2 fluxes that ranged from 0.17 to 0.37 tonnes 10 km^{-2} yr^{-1} (7.08×10^8 to 15.4×10^8 molecules cm^{-2} s^{-1}) at four sites in the Cairngorm mountain range, Scotland between 0 and –3.5 ^oC; measured mean NO_3^- concentrations at these sites were 4 mM. In comparison, our experiments reveal NO_2 fluxes during the isothermal and temperature-programmed photolysis of $[NO_3^-]_o$ = 50 mM nitrate at –4 ^oC, ranging from ~ 6.0×10^8 to ~ 45×10^8 molecules cm^{-2} s^{-1}. Although this difference is nonlinear, the factor of ~ 3 difference between our NO_2 fluxes measured in the laboratory and Fisher *et al.*[54] NO_2 flux measurements in the field are due to us using greater initial concentrations (e.g., factor ~13).

Since NO_3^-, HCHO, and HOOH concentrations within ice cores have been used to infer paleoatmospheric conditions,[57-59] their photolytic losses before encapsulation in deeper polycrystalline ice need to be considered. Furthermore, $^{\cdot}OH$ produced directly from H_2O_2 and NO_3^- photolysis in snow and ice is capable of oxidizing higher molecular weight organic compounds to produce aldehydes (e.g., HCHO)[19,20] and other oxidized organic products as reported by Dubowski and Hoffmann[60] in addition to photodecarboxylation of compounds such as pyruvic acid to yield CO_2.

Conclusions

Thermograms of NO and NO_2 during the photolysis of $[NO_3^-]_o$ = 50 mM between $-30 \leq T/°C \leq 5$ imply that NO molecules, starting at lower temperatures, preferentially partition to air from the QLL and its movement is faster in subsurficial water channels (or veins) in polycrystalline ice matrices upon warming, compared to NO_2 molecules. This phenomenon exemplifies qualitatively how the ice matrix behaves as a filter or molecular sieve for gases, such as NO and NO_2. The temperature dependence NO and NO_2's Henry's law coefficients and their ice-air partition coefficients relative to each corroborates our inference. NO desorption profiles at ∂H = 0.70 and 0.10 $^oC\ min^1$ reveal that NO_2^- photolysis governs the production NO before NO_2^- reaches steady-state, where after, NO_2 photolysis dictates NO production.

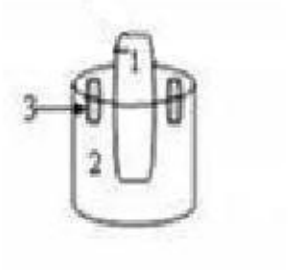

(a)

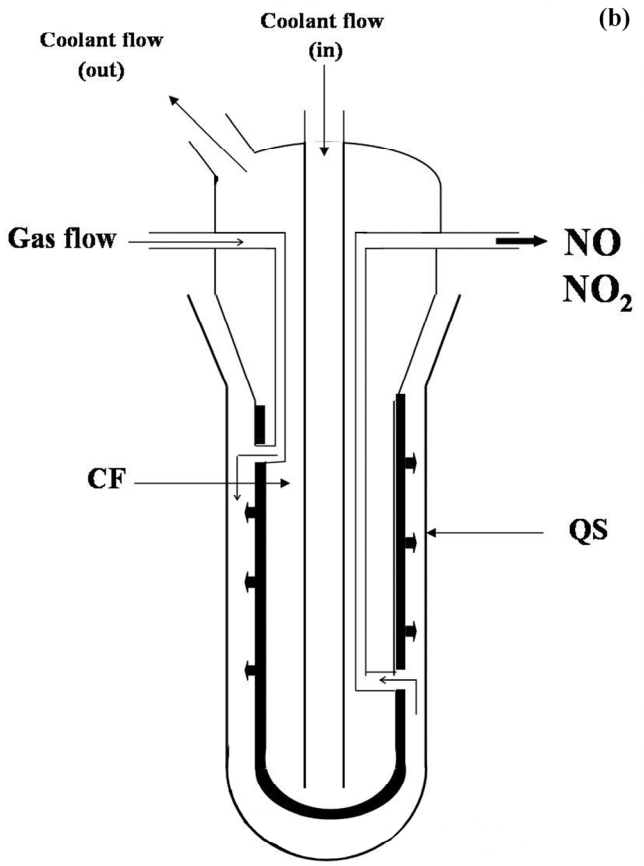

Figure 6.1. (a) (1) photolysis cell (see Figure 6.1 (b)); (2) reflective reaction chamber; (3) pen-ray UV lamps emitting at $\lambda_{max} \approx 313$ nm. (b) The reaction cell, CF: coldfinger ; QS: quartz sheath.

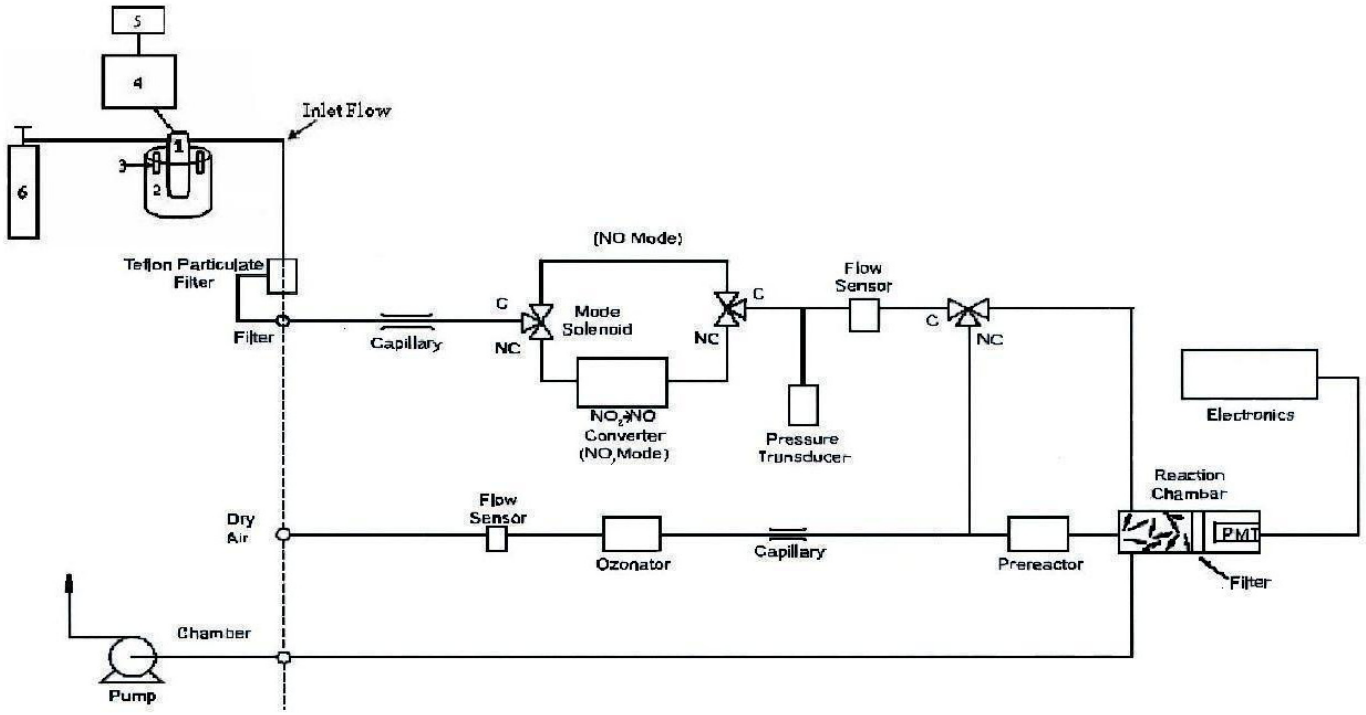

Figure 6.2. . Schematic diagram of the experimental setup. (1) Photolysis cell (see Figure 6.1); (2) reflective reaction chamber; (3) pen-ray UV lamps emitting at $\lambda_{max} \approx 313$ nm; (4) circulating cryostat; (5) computer workstation utilizing Thermo Neslab Nescom software; (6) Zero air carrier gas. Thermo Electron Corporation, Model 42C-TL NO-NO_2-NO_x Analyzer flow scheme shows that sample gas enters through a flow control capillary and was directed to the NO control solenoid. Sample gas was then routed to the prereactor where it reacted with ozone before the reaction chamber to give a dynamic zero reading for the analyzer or was sent to the prereactor solenoid where it was sent directly through the valve to the reaction chamber where it missed with ozone to give an NO reading.

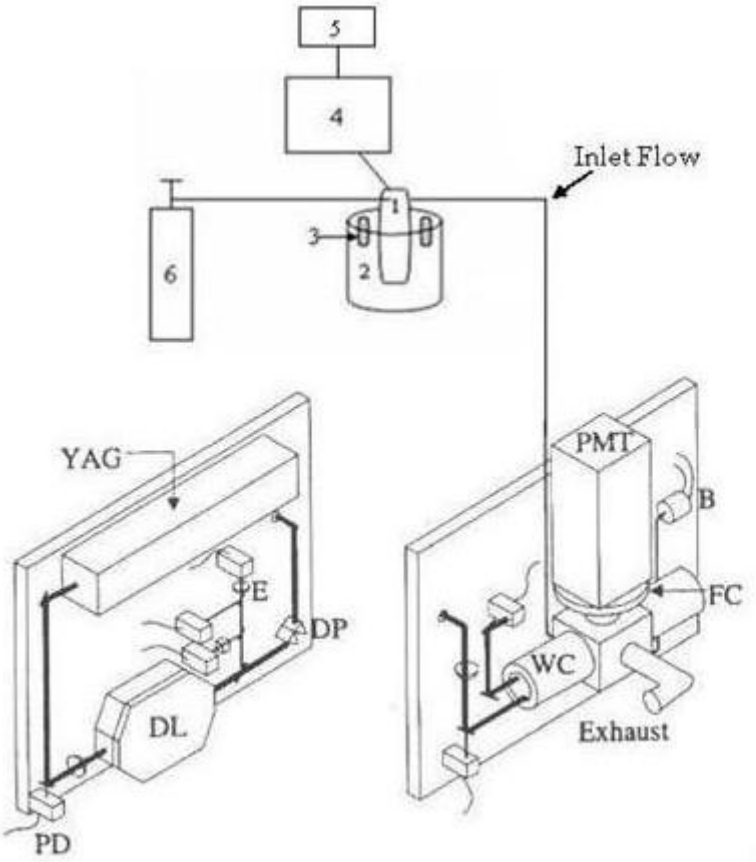

Figure 6.3. Schematic diagram of the experimental setup. (1) photolysis cell (see Figure 6.1); (2) reflective reaction chamber; (3) pen-ray UV lamps emitting at $\lambda_{max} \approx 313$ nm; (4) circulating cryostat; (5) computer workstation utilizing Thermo Neslab Nescom software; (6) Zero air carrier gas. Schematic of the UC, Berkeley laser-induced fluorescence NO_2 instrument was extracted with modifications from Thornton et al. (2000). The core of the instrument is mounted on a breadboard, one side holding the laser subsystem and the other side the detection axis. A frequency doubled Nd^{3+}:YAG laser (YAG) at 532 nm pumps a custom-built dye laser (DL), the output (585 nm) of which is sampled by fused silica beam splitters to monitor power, frequency (by measuring transmittance through an NO_2 reference cell shown as a cube), and line width measured with an external etalon (E). Six photodiode detectors (PD) are used to measure laser power at various points along the beam path. A set of dispersion prisms (DP) is used to separate the 585 nm light from the 532 nm light which is then dumped. The 585 nm light is then sent through a hole in the breadboard to the detection side to the multipass White Cell (WC). The pressure in the WC is measured with a manometer., 100 Torr Baratron (B). NO_2 fluorescence is collected and sent through a series of optical filters housed in the filter changer (FC) to the photomultiplier tube in its TE-cooled housing (PMT).

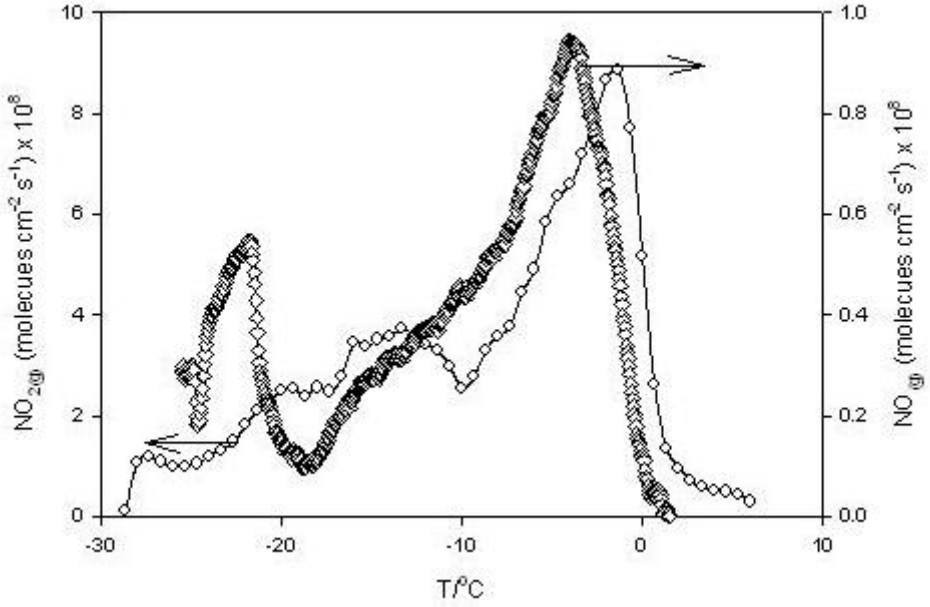

Figure 6.4a.: ◊: NO; O: NO_2, released during a 0.70 $^oC\ min^{-1}$ ramp rate from irradiated 50 mM nitrate-doped polycrystalline ice vs. temperature.

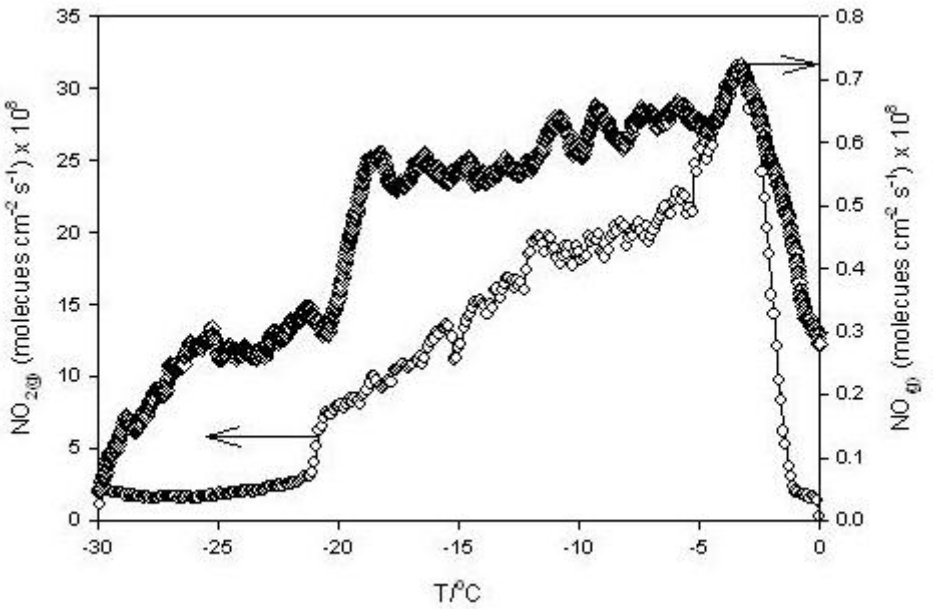

Figure 6.4b.: ◊: NO; O: NO_2, released during a 0.10 $^oC\ min^{-1}$ ramp rate from irradiated 50 mM nitrate-doped polycrystalline ice vs. temperature.

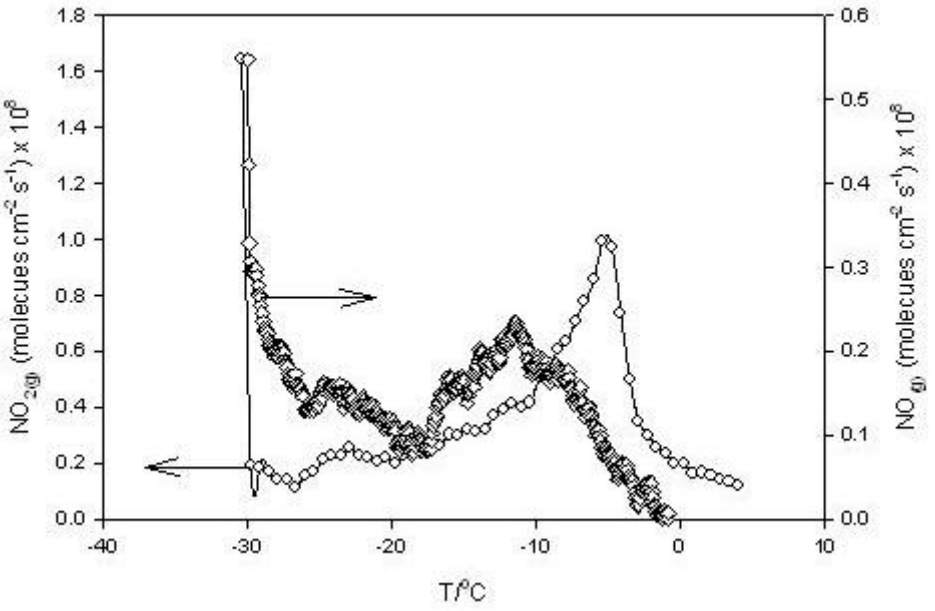

Figure 6.5.: ◊: NO; O: NO_2, released during a 0.70 ^{o}C min^{-1} ramp rate (without photolysis) after 3 hour irradiation of 50 mM nitrate-doped polycrystalline at -30 ^{o}C.

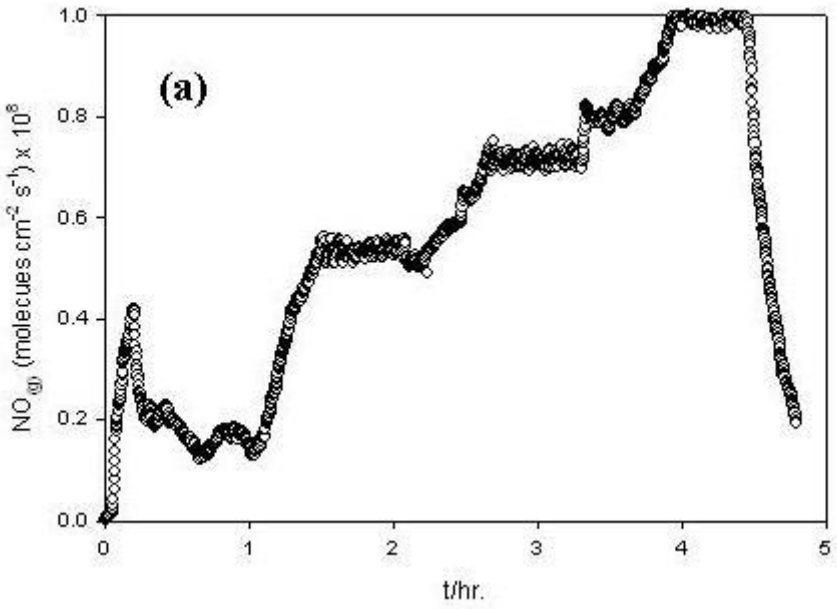
(a)
$NO_{@}$ (molecues cm^{-2} s^{-1}) x 10^{8}
t/hr.

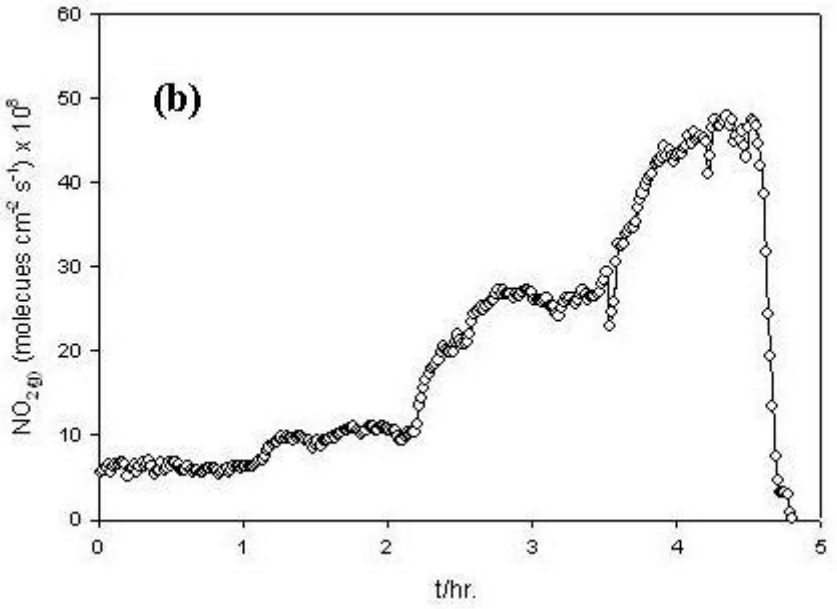
(b)
$NO_{2@}$ (molecues cm^{-2} s^{-1}) x 10^{8}
t/hr.

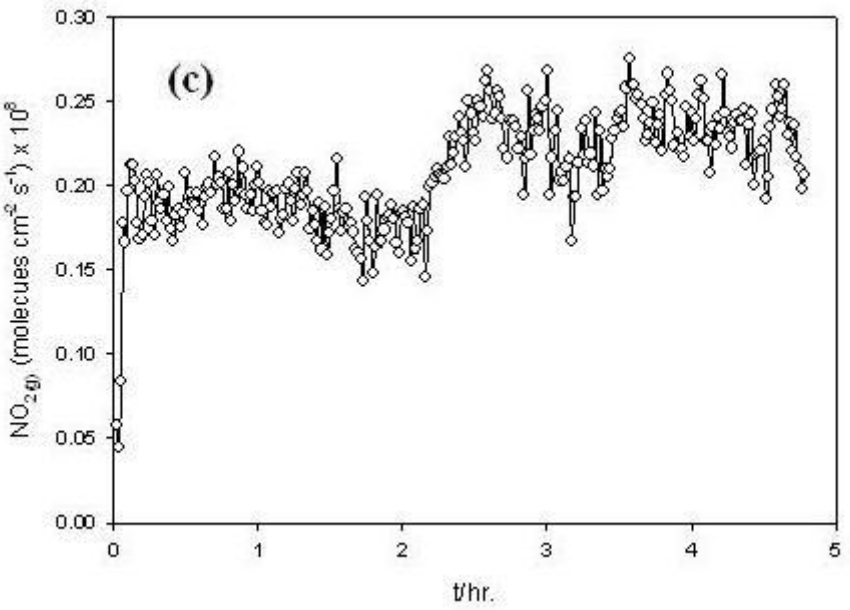

Figure 6.6. (a) NO released during the photolysis of 50 mM nitrate-doped polycrystalline ice with 0.70 ^{o}C min^{-1} ramp rate at -30 ≤ T/^{o}C ≤ 5; isothermal experiments were conducted for 1 hour at -30, -20, 10, and -4 ^{o}C with photolysis between ramps. (b) NO_2 released during the photolysis of 50 mM nitrate-doped polycrystalline ice with 0.70 ^{o}C min^{-1} ramp rate at -30 ≤ T/^{o}C ≤ 5; isothermal experiments were conducted for 1 hour at -30, -20, 10, and -4 ^{o}C with photolysis between ramps. (c) NO_2 released during the photolysis of 2 μM nitrate-doped polycrystalline ice with 0.70 ^{o}C min^{-1} ramp rate at -30 ≤ T/^{o}C ≤ 5; isothermal experiments were conducted for 1 hour at -30, -20, -10, and -4 ^{o}C with photolysis between ramps.

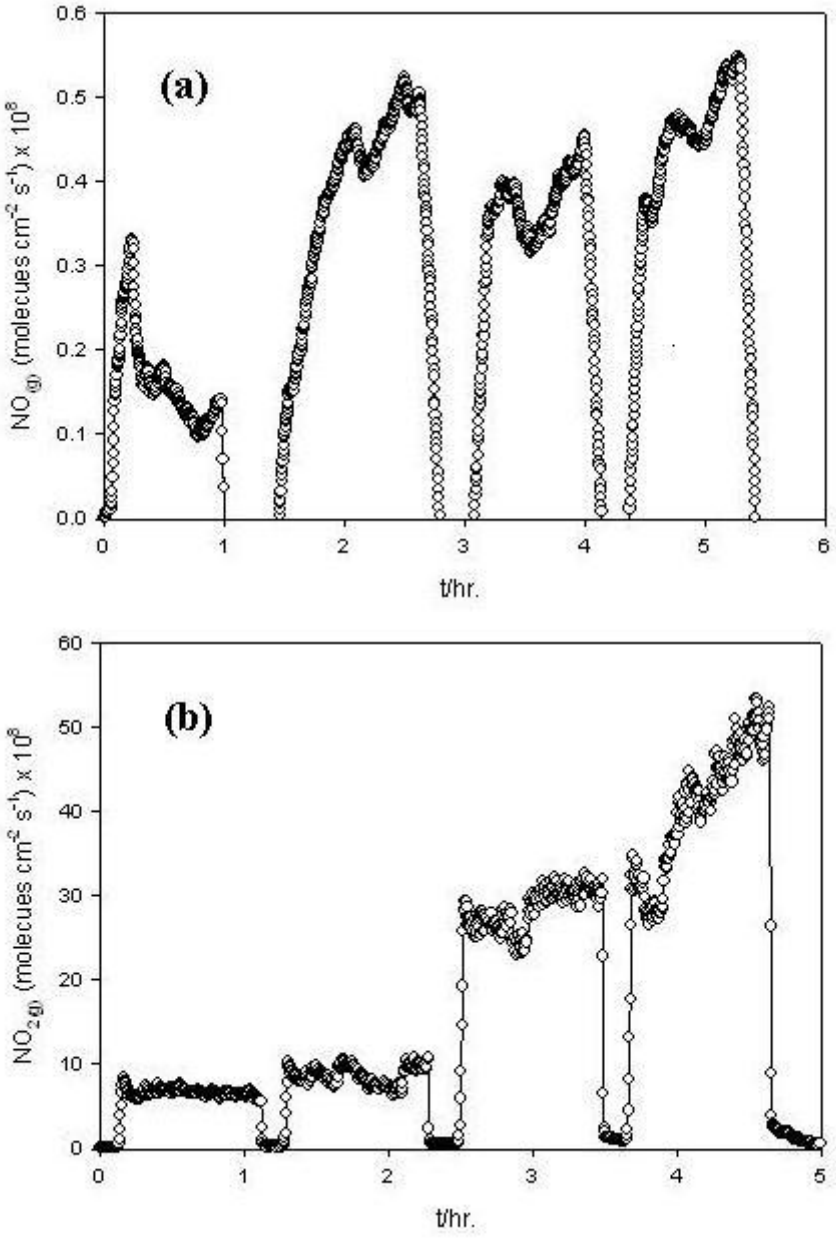
(a)
$NO_{(g)}$ (molecues cm^{-2} s^{-1}) x 10^8
t/hr.
(b)
$NO_{2(g)}$ (molecues cm^{-2} s^{-1}) x 10^8
t/hr.

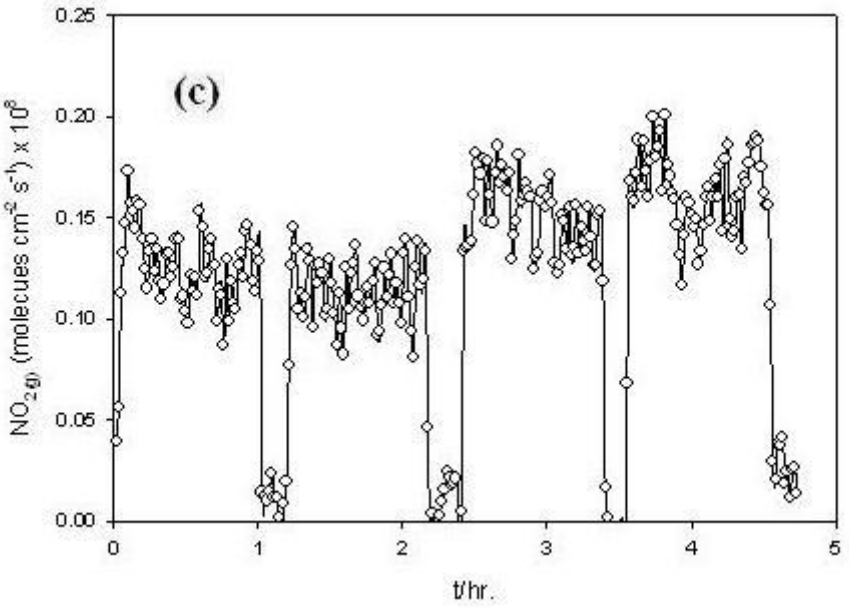

Figure 6.7. (a) NO released during the photolysis of 50 mM nitrate-doped polycrystalline ice with 0.70 ^{o}C min^{-1} ramp rate at -30 ≤ T/^{o}C ≤ 5; isothermal experiments were conducted for 1 hour at -30, -20, 10, and -4 ^{o}C without photolysis between ramps. (b) NO_2 released during the photolysis of 50 mM nitrate-doped polycrystalline ice with 0.70 ^{o}C min^{-1} ramp rate at -30 ≤ T/^{o}C ≤ 5; isothermal experiments were conducted for 1 hour at -30, -20, 10, and -4 ^{o}C without photolysis between ramps. (c) NO_2 released during the photolysis of 2 μM nitrate-doped polycrystalline ice with 0.70 ^{o}C min^{-1} ramp rate at -30 ≤ T/^{o}C ≤ 5; isothermal experiments were conducted for 1 hour at -30, -20, 10, and -4 ^{o}C without photolysis between ramps.

References

(1) Platt, U. *The Origin of Nitrous and Nitric Acid in the Atmosphere*; Springer-Verlag: New York, **1986**; Vol. G6.

(2) Logan, J. A. *J. Geophys. Res.* **1983**, *88*, 10785.

(3) Mulvaney, R.; Wagenbach, D.; Wolff, E. W. *J. Geophys. Res.* **1998**, *103*, 11021.

(4) Legrand, M.; Mayewski, P. *Rev. Geophys.* **1997**, *35*, 219.

(5) Dibb, J. E.; Talbot, R. W.; Munger, J. W.; Jacob, D. J.; Fan, S. M. *J. Geophys. Res.* **1998**, *103*, 3475.

(6) Wolff, E. W. *Nitrate in Polar Ice*; Springer-Verlag: New York, 1995; Vol. I30.

(7) Beine, H. J.; Domine, F.; Ianniello, A.; Nardino, M.; Allegrini, I.; Teinila, K.; Hillamo, R. *Atmos. Chem. Phys.* **2003**, *3*, 335.

(8) Beine, H. J.; Domine, F.; Simpson, W.; Honrath, R. E.; Sparapani, R.; Zhou, X. L.; King, M. *Atmos. Environ.* **2002**, *36*, 2707.

(9) Beine, H. J.; Honrath, R. E.; Domine, F.; Simpson, W. R.; Fuentes, J. D. *J. Geophys. Res.* **2002**, *107*.

(10) Dibb, J. E.; Arsenault, M.; Peterson, M. C.; Honrath, R. E. *Atmos. Environ.* **2002**, *36*, 2501.

(11) Honrath, R. E.; Lu, Y.; Peterson, M. C.; Dibb, J. E.; Arsenault, M. A.; Cullen, N. J.; Steffen, K. *Atmos. Environ.* **2002**, *36*, 2629.

(12) Davis, D.; Nowak, J. B.; Chen, G.; Buhr, M.; Arimoto, R.; Hogan, A.; Eisele, F.; Mauldin, L.; Tanner, D.; Shetter, R.; Lefer, B.; McMurry, P. *Geophys. Res. Lett.* **2001**, *28*, 3625.

(13) Peterson, M. C.; Honrath, R. E. *Geophys. Res. Lett.* **2001**, *28*, 511.

(14) Jones, A. E.; Weller, R.; Wolff, E. W.; Jacobi, H. W. *Geophys. Res. Lett.* **2000**, *27*, 345.

(15) Ridley, B.; Walega, J.; Montzka, D.; Grahek, F.; Atlas, E.; Flocke, F.; Stroud, V.; Deary, J.; Gallant, A.; Boudries, H.; Bottenheim, J.; Anlauf, K.; Worthy, D.; Sumner, A. L.; Splawn, B.; Shepson, P. *J. Atmos. Chem.* **2000**, *36*, 1.

(16) Honrath, R. E.; Peterson, M. C.; Dziobak, M. P.; Dibb, J. E.; Arsenault, M. A.; Green, S. A. *Geophys. Res. Lett.* **2000**, *27*, 2237.

(17) Chu, L.; Anastasio, C. *J. Phys. Chem. A.* **2003**, *107*, 9594.

(18) Honrath, R. E.; Peterson, M. C.; Guo, S.; Dibb, J. E.; Shepson, P. B.; Campbell, B. *Geophys. Res. Lett.* **1999**, *26*, 695.

(19) Domine, F.; Shepson, P. B. *Science* **2002**, *297*, 1506.

(20) Sumner, A. L.; Shepson, P. B. *Nature* **1999**, *398*, 230.

(21) Boxe, C. S.; Colussi, A. J.; Hoffmann, M. R.; Tan, D.; Mastromarino, J.; Case, A. T.; Sandholm, S. T.; Davis, D. D. *J. Phys. Chem. A.* **2003**, *107*, 11409.

(22) Dubowski, Y.; Colussi, A. J.; Boxe, C.; Hoffmann, M. R. *J. Phys. Chem. A.* **2002**, *106*, 6967.

(23) Dubowski, Y.; Colussi, A. J.; Hoffmann, M. R. *J. Phys. Chem. A.* **2001**, *105*, 4928.

(24) Tombari, E.; Salvetti, G.; Ferrari, C.; Johari, G. P. *J. Chem. Phys.* **2005**, *122*, 104712.

(25) Boxe, C. S.; Colussi, A. J.; Hoffmann, M. R.; Murphy, J.; Wooldridge, P. J.; Betram, T.; Cohen, R. C. Photochemical Production and Release of Gaseous NO2 From Nitrate-doped Water Ice. In *J. Phys. Chem. A.*, (*submitted*) **2005**.

(26) Mizuno, Y.; Wakahama, G. *J. Phys. Chem.* **1983**, *87*, 4161.

(27) Calvert, J.; Pitts, J. N. *Photochemistry*; Wiley: New York, **1966**.

(28) Clough, P. N.; Thrush, B. A. *Trans. Faraday Soc.* **1967**, *63*, 915.

(29) Thornton, J. A.; Wooldridge, P. J.; Cohen, R. C. *Anal. Chem.* **2000**, *72*, 528.

(30) Gaffney, J. S.; Marley, N. A.; Cunningham, M. M. *Environ. Sci. Technol.* **1992**, *26*, 207.

(31) Maria, H. J.; McDonald, J. R.; McGlynn, S. P. *J. Am. Chem. Soc.* **1973**, *95*, 1050.

(32) Meyerste.D; Treinin, A. *Trans. Faraday Soc.* **1961**, *57*, 2104.

(33) Meyerste.D; Treinin, A. *Bull. Res. Counc. Isr.* **1961**, *A 10*, 39.

(34) Mack, J.; Bolton, J. R. *J. Photochem. Photobiol. A-Chem.* **1999**, *128*, 1.

(35) Mark, G.; Korth, H. G.; Schuchmann, H. P.; vonSonntag, C. *J. Photochem. Photobiol. A-Chem.* **1996**, *101*, 89.

(36) Daniels, M.; Meyers, R. V.; Belardo, E. V. *J. Phys. Chem.* **1968**, *72*, 389.

(37) Jankowski, J. J.; Kieber, D. J.; Mopper, K. *Photochem. Photobiol.* **1999**, *70*, 319.

(38) Warneck, P.; Wurzinger, C. *J. Phys. Chem.* **1988**, *92*, 6278.

(39) Zuo, Y. G.; Deng, Y. W. *Chemosphere* **1998**, *36*, 181.

(40) Rotlevi, E.; Treinin, A. *J. Phys. Chem.* **1965**, *69*, 2645.

(41) McEwen, K. L. *J. Chem. Phys.* **1961**, *34*, 547.

(42) McConnell, H. *J. Chem. Phys.* **1952**, *20*, 700.

(43) Bartels-Rausch, T.; Eichler, B.; Zimmermann, P.; Gaggeler, H. W.; Ammann, M. *Atmos. Chem. Phys.* **2002**, *2*, 235.

(44) Wettlaufer, J. S. *Phys. Rev. Lett.* **1999**, *82*, 2516.

(45) De Angelis, D.; Legrand, M. *Ice Core Studies of Global Biogeochemical Cycles, NATO ASI Ser., Ser. 1* **1995**, *30*, 361.

(46) Silvente, E.; Legrand, M. *Ice Core Studies of Global Biogeochemical Cycles, NATO ASI Ser., Ser. 1* **1995**, *30*, 225.

(47) Jaffe, D. A.; Zukowski, M. D. *Atmos. Environ.* **1993**, *27*, 2935.

(48) Stottlemyer, R.; Toczydlowski, D. *Can. J. Fish. Aquat. Sci.* **1990**, *47*, 290.

(49) Cotter, E. S. N.; Jones, A. E.; Wolff, E. W.; Bauguitte, S. J. B. *J. Geophys. Res.-Atmos.* **2003**, *108*.

(50) Jacobi, H. W.; Bales, R. C.; Honrath, R. E.; Peterson, M. C.; Dibb, J. E.; Swanson, A. L.; Albert, M. R. *Atmos. Environ.* **2004**, *38*, 1687.

(51) Anastasio, C.; Jordan, A. L. *Atmos. Environ.* **2004**, *38*, 1153.

(52) Vaghjiani, G. L.; Turnipseed, A. A.; Warren, R. F.; Ravishankara, A. R. *J. Chem. Phys.* **1992**, *96*, 5878.

(53) Vaghjiani, G. L.; Ravishankara, A. R. *J. Chem. Phys.* **1990**, *92*, 996.

(54) Fisher, F. N.; King, M. D.; Lee-Taylor, J. *J. Geophys. Res.* **2005**.

(55) Kang, S. C.; Mayewski, P. A.; Qin, D. H.; Sneed, S. A.; Ren, J. W.; Zhang, D. Q. *Atmos. Environ.* **2004**, *38*, 2819.

(56) Hidy, G. M. *Atmos. Environ.* **2003**, *37*, 1231.

(57) Sigg, A.; Neftel, A. *Nature* **1991**, *351*, 557.

(58) Staffelbach, T.; Neftel, A.; Stauffer, B.; Jacob, D. *Nature* **1991**, *349*, 603.

(59) Mayewski, P. A.; Legrand, M. R. *Nature* **1990**, *346*, 258.

(60) Dubowski, Y.; Hoffmann, M. R. *Geophys. Res. Lett.* **2000**, *27*, 3321.

(61) Moore, W. J. *Physical Chemistry*, 3rd ed.; Prentice Hall: Englewood Cliffs, **1962**.